HHS Public Access

Author manuscript

Health Phys. Author manuscript; available in PMC 2016 November 01.

Published in final edited form as:

Health Phys. 2015 November ; 109(5): 479–492. doi:10.1097/HP.0000000000000344.

The Evolving MCART Multimodal Imaging Core: Establishing a protocol for Computed Tomography and Echocardiography in the Rhesus macaque to perform longitudinal analysis of radiation-induced organ injury

Eduardo B. de Faria[*], **Kory R. Barrow**[‡], **Bradley T. Ruehle**[¥], **Jordan T. Parker**[‡], **Elisa Swartz**[¥], **Cheryl Taylor-Howell**[‡], **Kaitlyn M. Kieta**[‡], **Cynthia J. Lees**[§], **Meg M. Sleeper**[‡], **Travis Dobbin**[‡], **Adam D. Baron**[¥], **Pranshu Mohindra**[†], and **Thomas J. MacVittie**[†]

[*] University of Maryland, School of Medicine, Dept. of Radiation Oncology, Preclinical Radiobiology Laboratory, Echocardiography and Computed Tomography Team

[‡] University of Maryland, School of Medicine, Dept. of Radiation Oncology, Preclinical Radiobiology Laboratory, Computed Tomography Team, Department of Small Animal Clinical Sciences, College of Veterinary Medicine, Gainesville, Florida

[¥] University of Maryland, School of Medicine, Dept. of Radiation Oncology, Preclinical Radiobiology Laboratory, Echocardiography Team

[§]Department of Pathology, Section on Comparative Medicine, Wake Forest School of Medicine, Winston-Salem, NC

[†] University of Maryland, School of Medicine, Department of Radiation Oncology, Baltimore, MD

Abstract

Computed Tomography (CT) and Echocardiography (EC) are two imaging modalities that produce critical longitudinal data that can be analyzed for radiation-induced organ-specific injury to the lung and heart. The Medical Countermeasures Against Radiological Threats (MCART) consortium has a well-established animal model research platform that includes nonhuman primate (NHP) models of the acute radiation syndrome and the delayed effects of acute radiation exposure. These models call for a definition of the latency, incidence, severity, duration, and resolution of different organ-specific radiation-induced subsyndromes. The pulmonary subsyndromes and cardiac effects are a pair of inter-dependent syndromes impacted by exposure to potentially lethal doses of radiation. Establishing a connection between these will reveal important information about their interaction and progression of injury and recovery. Herein, we demonstrate the use of CT and EC data in the rhesus macaque models to define delayed organ injury thereby establishing: a) consistent and reliable methodology to assess radiation-induced damage to the lung and heart, b) an extensive database in normal age-matched NHP for key primary and secondary endpoints, c) identified problematic variables in imaging techniques and

For correspondence contact: Eduardo Faria, 10 S. Pine St. MSTF 6-00B, Baltimore, MD 21201, Office: (410) 706-5282, Fax: (410) 706-5270 or efaria@som.umaryland.edu.

The authors declare no conflict of interest.

proposed solutions to maintain data integrity and d) initiated longitudinal analysis of potentially lethal radiation-induced damage to the lung and heart.

Keywords

diagnostic imaging; laboratory animals; radiation damage; respiratory system

INTRODUCTION

The MCART consortium is charged with developing medical countermeasures (MCM) against the acute radiation syndrome (ARS) and the delayed effects of acute radiation exposure (DEARE). The purpose of this translational research is to define the pathophysiological mechanism of radiation injury, determine the efficacy of MCM, and identify the mechanisms of action of radiation-induced organ-specific effects and their mitigation by MCM while adhering to the “animal rule” criteria of recent FDA guidance documents (Crawford and FDA 2002; Food and Drug Administration 2014). MCART established a rhesus macaque animal model research platform that allows the integration of models focused on organ-specific and multi-organ injury (MOI) of the ARS and DEARE. The FDA guidance document includes recommendations to utilize the appropriate study duration for each subsyndrome and to determine the natural history for key organ damage of the ARS and DEARE. Analysis of evolving radiation subsyndromes requires that a longitudinal analysis be performed where organ-specific information is collected throughout the time course of the radiation-induced sequelae. Further, organ-specific longitudinal analysis can establish a link between the dose- and time-dependent evolution of the ARS and DEARE. The lung and heart are two organs that display characteristics of DEARE. The MCART recently organized its research platform to permit the longitudinal analysis of these organ sequelae over the time course from acute radiation exposure to time of onset, progression and resolution of organ dysfunction. In addition to the independent effects of radiation-induced lung and heart injury, there are also indirect effects of injury to one organ impacting the function of the other, often worsening the radiation effect. The concomitant irradiation of the heart is an additional risk factor for radiation-induced lung damage (Ghobadi et al. 2012; van Luijk et al. 2005). Van Luijk et al suggested that exposure of the heart reduced the tolerance of the lung for radiation-induced injury and furthermore the irradiated heart had an early damage component that may occur concomitantly with the latent phase of lung injury. Co-irradiation of the heart enhances early radiation-induced lung function loss when compared to heart or lung irradiation alone (van Luijk et al. 2005). Irradiation of the lung can induce pulmonary hypertension, edema, pneumonitis and fibrosis which may indirectly cause left ventricle diastolic dysfunction due to congestion in the cardiopulmonary circuit. Direct radiation of the heart affects cardiac vasculature and myocardium to cause left ventricle diastolic dysfunction, which in turn promotes pulmonary interstitial edema. Both dose-dependent mechanisms are activated when co-irradiation occurs which can result in biventricular dysfunction and aggregate the impact of radiation injury (Ghobadi et al. 2012).

The NHP whole thorax lung irradiation (WTLI) and partial body irradiation with 2.5% bone marrow sparing (PBI/BM2.5) models provide an unparalleled opportunity to assess the interaction of lung and heart in combined organ injury. The MCART multi-modal imaging core is focused on exploring the potential of non-invasive imaging to perform longitudinal analysis of radiation induced lung (pulmonary-DEARE) and heart (cardiac-DEARE) damage and assess MCM efficacy.

Computed tomography (CT) and echocardiography (EC) are two non-invasive imaging modalities with relative and cumulative benefits in evaluating organ-specific damage. CT will be critical in evaluating the physiological morphology of the lungs by establishing density ranges that are indicative of various radiation-induced injuries such as pneumonitis, fibrosis, and pleural and pericardial effusions. EC will be essential in studying ventricular anatomy and physiology, valve function, blood flow, and cardiac musculature in an effort to define the time course of acute radiation-induced cardiac-DEARE. In the case of pulmonary-DEARE, longitudinal changes in clinical parameters such as respiratory rate and saturation of peripheral oxygen (SpO_2) can be linked to lung pathology observed using the chest CT images. Unraveling the connection between the heart and lung pathology is paramount in identifying the cause and effect relationships in these organ systems. The MCART tissue imaging core provides organ-specific imaging using matrix assisted laser desorption-ionization (MALDI), and mass spectrometry imaging (MSI) to further characterize organ histology and also identify possible biomarkers associated with radiation injury as well as organ histology (Scott et al. 2014; Jones et al. 2014; Carter et al. 2015). Although these techniques are only performed on tissue samples collected at necropsy, they provide a clear cellular link to organ imaging which can be correlated with non-invasive imaging performed at corresponding time points along the entire study duration.

The observation of lung and heart damage over the entire time course of injury development and treatment with medical management and MCM will allow further definition of the relationships between the ARS and DEARE in the rhesus macaque model and identify a link between the two organ systems (Ghobadi et al. 2012; van Luijk et al. 2005). The purpose of this paper is to a) report standardized methods for CT and EC-based longitudinal analysis of radiation-induced lung and heart injury in the NHP, b) identify primary and secondary endpoints for evidence of organ-specific damage, c) establish a CT and EC database for the young rhesus macaque, and d) present an initial longitudinal data analysis of the time course of radiation-induced damage to the lung and heart.

MATERIALS AND METHODS

Animals

Computed tomography scans were performed on 40 normal male rhesus macaques, weighing from 4.7 to 9.1 kg, to establish baseline values. Of that number, 20 male rhesus macaques were later used in longitudinal irradiation studies. Echocardiograms were performed on 32 male rhesus macaques (*Macaca mulatta*) weighing from 5.0 to 6.8 kg. All animals were between three to four years old, healthy, negative for tuberculosis and herpes B virus, and seronegative for simian immunodeficiency virus, simian T cell leukemia virus type 1, and malaria. Animal housing and care were performed as previously described by

(MacVittie et al. 2012; Garofalo et al. 2014c). Complete physical examinations and complete blood counts were performed prior to the echocardiogram. All animals were acclimated to a supine restrain device prior the CT scan. All animal procedures were performed according to the approved University of Maryland Baltimore Institutional Animal Care and Use Committee (IACUC) protocol.

Anesthesia

Prior to physical examination, anesthesia was induced using ketamine hydrochloride (Ketaset®, 800 5th Street NW, Fort Dodge Animal Health, IA 50501); Ketasthesia®, Pfizer or Henry Schein Animal Health, Putney) (10± 5mg/kg −1 of the most recent body weight) intramuscularly (IM) in the quadriceps muscle using a ≤23 gauge needle according to the respective study protocol. During the echocardiogram examination, additional ketamine was administered IM to maintain sedation. Prior to CT scans and irradiation procedures, (0.5-1.01± 0.1mg/kg −1) Xylazine (AnaSed, Lloyd Laboratories, 604 West Thomas Avenue, Shenandoah, IA 51601) was administered IM.

Irradiation procedures

A 6 MV linear accelerator (LINAC) photon source (maximum photon energy of 6MV, average energy of approximately 2MV) was used to irradiate all animals. Animals in WTLI studies were irradiated to the whole thorax to a target, midline tissue dose of 10.74±0.15Gy, prescribed to midplane at the level of the xiphoid at a dose rate of 0.80 ± 0.10Gy/min. Irradiations were performed in an AP/PA technique with approximately 50% dose contribution from both the AP beam and the PA beam. Animals for PBI/BM2.5 studies were positioned such that the top of the head to the top half of the tibiae were positioned inside the beam field. The bottom half of the tibiae, ankles, feet and toes were positioned outside of the beam field. For PBI/BM2.5, the NHP were irradiated to a midline tissue does of 10.0Gy at a dose rate of 0.80 ± 0.10Gy/min.

Medical management

Medical management based on clinical signs is provided to all study animals as per a protocol approved by the institutional animal care and use committee (IACUC). Management includes corticosteroids, diuretics, anti-emetics, fluid support, antibiotics, anti-diarrheal, anti-ulcerative, and nutritional support. Dexamethasone (Henry Schein Animal Health, Dublin OH) was administered according to IACUC-approved “triggers-to-treat and –stop”, Furosemide (Hospira, Lake Forest, IL 60045) was administered by veterinary prescription only based on response to clinical observations. The administration of corticosteroids may be a confounding factor when analyzing data as they are known to influence the appearance of lung injury and have been suggested to prolong mean survival time and mitigate pleural effusions in mouse models of radiation-induced lung injury and rhesus macaques (Gross 1980; Gross et al. 1988; Garofalo et al. 2014a; Garofalo et al. 2014c; Geraci et al. 1992).

Computed tomography methodology

All CT images were acquired using a GE LightSpeed 2.X multi-slice CT scanner (GE Medical Systems, Inc, 3000 Grandview Boulevard, Waukesha, WI 53188, United States) without the aid of intravenous contrast media; slice thickness of 1.0-1.25 mm a 120-KV potential and a resolution of 0.853 pixels. Computed tomography scans were obtained prior to irradiation (baseline) and then acquired approximately every 30 days, starting at 30 days post irradiation (DPI). In specific studies, additional scans were acquired pre and post dexamethasone administration and only repeated should an additional course be required. When possible, CT scans were also performed on NHPs that meet euthanasia criteria prior to the study endpoint of 180 DPI (Garofalo et al. 2014b).

Scans were analyzed using the MIM® imaging software suite (MIM® Software Inc., 25200 Chagrin Boulevard, Suite 200, Cleveland, OH 44122) in a quantitative semi-automated method as described by Garofalo et al 2014 based on differences in morphology and radiodensity measured in Hounsfield Units (HU) (Garofalo et al. 2014b). Normal lung volume (NLV) was measured by selecting a “seed point” representative of normal lung and using the MIM® software’s “region grow” function to generate a contour based on normal lung HU limits (−880.0: −200.0). Portions that may have been falsely included in the lung boundaries (e.g., stomach, trachea) were manually excluded (Garofalo et al. 2014b). The contour was then manually edited to include normal regions of lung that may have been excluded by the region grow function, such as the pulmonary vessels and segmental bronchi. With this approach, the software excluded areas of pneumonitis/fibrosis (PF) from the auto-contour as any region with HU more than −200.0. Total lung volume (TLV) was then obtained by cloning the NLV and manually expanding the contour to the anatomic boundaries of the lungs including areas of PF. A contour of PF was created by subtracting NLV from TLV using MIM® software’s Boolean operations. Pleural effusions (PE) located outside of the lungs in the pleural space were identified by characteristic appearances (homogeneous in density, located in between lobes, and/or layering). These regions of PE were then manually contoured as a separate volume (Garofalo et al. 2014b). Unlike the HU range definition for normal lung, the HU range for pleural effusions is too variable to have an exact range. Further, the HU range approximates that of the soft-tissues of the chest wall making auto-segmentation challenging. Hence, we used the “HU Fat-Water-Tissue” anatomic viewing window available in the MIM® imaging software, which displays fatty tissues and deposits as yellow, water and other fluids as blue and tissues in green (Fig. 1). Similarly, pericardial effusions (PCE) were identified as shadowing around heart tissue by adjusting the viewing window of the CT scan and by using the Fat-Water-Tissue viewing window as above. . All volumes were presented as ratios compared against the TLV for each scan (eg., PF:TLV, PE:TLV) to eliminate variability that occurs between scans due to lack of breath holding techniques, size differences between NHPs, and any growth that may occur over the 180 day period (Garofalo et al. 2014b). Completed scans are reviewed and verified by at least one additional analyst to ensure accuracy and consistency between analysts.

Echocardiography (EC) methodology

After sedation, subjects were positioned on an acrylic “cut-out exam table” over a heated warming blanket in right and left lateral recumbency depending on the echocardiographic view being obtained. During the echocardiographic procedure SpO_2, body temperature, and respiratory rate were measured every 15 minutes. A three lead, noninvasive ECG was attached to the subject to monitor and record electrical activity of the heart and was used for timing of cardiac events during data analysis. Ultrasound System Philips CX50 (Philips Ultrasound, 22100 Bothell-Everett Highway, Bothell, WA 98021-8431) and Philips S8-3 transducer with a wavelength setting of 115Hz were used to acquire standard 2-dimensional (2D), motion mode (M-Mode), pulsed wave spectral Doppler (PW) and color-flow mapping echocardiographic images.

Echocardiography analysis

The images were processed on the work station Ultrasound System Philips CX50 (Philips Ultrasound, 22100 Bothell-Everett Highway, Bothell, WA 98021-8431) with the aid of Philips Q-Lab analysis software. All the exams were stored on digital media for subsequent analysis. Each measurement reported represents the calculated average from three consecutive cycles. Standard 2D echocardiographic views on frozen B-mode, taken during diastole, using the right parasternal short axis view at the level of left atrium and aorta were used to measure left atrial internal diameter (LA) and the aortic diameter (AO) (Hansson et al., 2002). The QLab software calculated automatically LA:Ao ratio. Thickness of the interventricular septum during diastole (IVSd) and systole (IVSs), left ventricular internal diameter in diastole (LVIDd) and systole (LVIDs), thickness of the left ventricular posterior wall in diastole (LVPWd) and in systole (LVPWs) using the leading edge to leading edge technique, were measured using targeted M-mode from the parasternal short-axis at the level of the mitral valve leaflet tips (Lang et al., 2015). The beginning of the QRS wave was used for timing diastolic measurements and the systolic measurement coincided with the smallest chamber diameter. Targeted M-mode was used at the level of the mitral valve to obtain the distance between the E-point septal separation (EPSS) of the mitral valve and interventricular septum. A three second loop from the apical four chamber view was taken to obtain the left ventricle chamber volume in diastole and systole (Lang et al., 2015). The machine automatically calculated left ventricular ejection fraction (EF) and fractional shortening (FS) from these values. A pulsed wave Doppler recording was obtained at the aortic root and the aortic peak flow velocity (AVmax) was measured. At the tips of the mitral valve leaflets, the left ventricular inflow velocities (MV peak A, MV peak E) were obtained with pulsed wave Doppler. The pulmonary valve peak outflow velocity and pressure gradient (PV Vmax, PV Vmax PG) were obtained in the short axis view at the pulmonary valve level (Quiñones et al., 2002).

RESULTS

Computed tomography: baseline values and imaging

Baseline values were established using CT scans from 40 naive NHP. The values include the mean of average HU values for each NHP’s lungs and average TLV as well as standard deviations and data ranges for each (Table 1). Our conventional approach to define normal

lung volume (NLV) was based on using the threshold range from −880 to −200 (Garofalo et al. 2014b). However, using the same cut-off to define radiological changes of radiation-induced lung injury (RILI) leads to an underestimation of PF (Fig. 2). Hence, further studies are needed to better define a CT HU cut-off to delineate RILI. As an example, the mean of average HU value plus one standard deviation for each NHP's lungs was calculated to be −445 HU. Use of −445 as a cut-off allowed better segmentation of radiological changes of radiation injury from apparently normal looking lung (Fig. 3). We are investigating this further as an approach to quantify radiation-induced lung injury using CT scan changes as an end-point (Mohindra et al. 2015).

Computed tomography: evolution of radiographic changes

Images at the lung apex, mid, and base as labeled in figure 4 are used to illustrate the time of onset, severity, and progression of lung damage (Fig. 5a and b). Longitudinal radiographic images from two representative NHP exposed to lethal WTLI (LD70/180); a surviving NHP euthanized at end of the 180d study duration and a non-survivor euthanized at 101 DPI are shown in Figs. 5a and 5b, respectively. These illustrate the development of PF and PE assessed every 30 days post exposure through the end of study or met early euthanasia criteria. Radiographic evidence of lung injury (PF, PE) evolved along the time course post exposure and provided radiographic evidence of the approximate time of onset, severity, and progression of pneumonitis/fibrosis and pleural effusion as well as the mitigating effect of dexamethasone administration. It is important to note that analysis of scans past 30 DPI are influenced by lethality and supportive care administration for more severely affected NHP. Results were reported as ratios (PF:TLV and PE:TLV), and represented the percentage of lung that appeared injured or acquired effusion at the time the CT scans were taken. The radiographic images show the presence of PF, PE and the use of dexamethasone and furosemide.

Pneumonitis/fibrosis (PF): incidence, severity, duration

Radiographic evidence of lung injury was first observed in 20.0% of the CT scans at 30 DPI and climbed to 100% of the 120 DPI CT scans and remained at 100.0% of scans through 180 DPI (Table 2). All 20 controls, irradiated macaques, with the exception of a single early mortality (d56), developed PF at some point in the study. Mean onset for observation of PF was calculated at 71 DPI with a median of 60 DPI. When present, values of PF ranged from a low of 0.02% at 60 DPI to a high of 17.69% at 120 DPI. Mean PF:TLV values peaked at 120 DPI.

Pleural effusion (PE): incidence, severity, duration

The first observed incidence of PE was at 30 DPI. Sixty percent (60.0%) of CT scans were positive. PE continued to be observed through the 180d study duration, with a low of 23.1% of positive CT scans noted at 90 DPI (Table 2). Seventeen of the 20 rhesus macaques developed PE at some point in the study. When present, the mean amount of PE was 23.54 mL, range 0.06 – 212.90 mL. Due to the exposure to potentially lethal doses of radiation, in some situations the volume of PE, which occupies the extra-parenchymal space, exceeded the TLV (Figure 1). The values of PE:TLV ranged from 0.02% to 178.35%. The mean

PE:TLV value peaked at 60 DPI and persisted in larger quantities through 90- 120 DPI. Mean onset for observation of PE was calculated at 51 DPI with a median of 31 DPI.

Pericardial effusion (PCE): incidence post WTLI

Observable amounts of PCE were present on 37.5% of CT scans at 60 DPI, 15.4% at 90DPI and 9.1% at 120 DPI (Table 2). Pericardial effusion was only present in eight rhesus macaques over the entire study duration. The amount of PCE ranged from 5.70 mL to 25.87 mL. The mean onset for observation of PCE was calculated at 68 DPI with a median of 60 DPI.

Echocardiography: baseline values and imaging

Initial EC established a database of baseline values for un-irradiated, naïve rhesus macaques (n=32). The mean values, standard deviations, data ranges, and correlation coefficients are presented for left ventricular function, left ventricular chamber geometry, and Doppler echocardiographic parameters (Tables 3-5). Standard baseline echocardiographic views are shown in Fig. 7. These parameters were chosen to provide a requisite primary database for analysis of radiation-induced cardiac damage. Changes in anatomy and physiology that characterize the cardiac-DEARE are likely to occur within these parameters and also provide information about the cardiac interaction with the pulmonary-DEARE.

Echocardiography: radiation-induced effects on the heart

Exams were performed between zero to 180 DPI following either 10.74Gy WTLI or 10Gy PBI/BM2.5. The exposure protocols using the WTLI and PBI/BM2.5 had respective mortalities of 70% and 65% consequent to radiation-induced lung injury over the 180d study duration (MacVittie et al. 2012; Garofalo et al. 2014a). Initial results revealed a tendency towards biventricular hypertrophy, right ventricular and atrial dilation, and pericardial effusion (Figs. 8-9). Other abnormalities included aortic regurgitation (Fig. 10), severely reduced fractional shortening, left ventricle hypocontractility, and mitral valve thickening.

Making the connection: the lung and the heart

The objective of this study is to observe and characterize the organ-specific injuries to define the clinical and subclinical signs that make up the pulmonary- and cardiac-DEARE. As stated previously, lung and heart co-irradiation has been shown to be a risk factor in developing tissue injury in the cardiopulmonary circuit. Radiographic and clinical evidence of lung injury may be observed as early as 30 DPI and persisting to 180 DPI. However, the latent period for echocardiographic evidence of cardiac dysfunction appears to be delayed until 90 DPI, indicating that the mechanisms causing cardiac damage are slower to develop (Fig. 11). Between the heart and the lungs, it is unclear which organ is affected first, if that organ causes primary damage to the other, or whether damage occurs simultaneously in both organs causing a cumulative effect. Left ventricular hypertrophy is a common injury associated with irradiation and is a relevant parameter to measure over time (Table 6). This type of cardio myopathy can lead to diastolic dysfunction, which may cause eventual left heart failure. Furthermore, the increasing dilation of the right ventricle, which can indicate

increased pressure in the pulmonary circuit, can lead to right heart failure (Ghobadi et al. 2012; van Luijk et al. 2005).

Left ventricular dysfunction can lead to elevated pressure in the pulmonary circulation and ultimately, pulmonary edema. Radiation-induced pulmonary fibrosis and pneumonitis have been associated with dilation of the right ventricle and right heart failure (Ghobadi et al. 2012; van Luijk et al. 2005). The longitudinal analysis of concurrent organ damage over the time course of prolonged radiation damage provides a wealth of information relative to the underlying physiology of each organ and their potential interaction. Pairing this with other post-necropsy tissue imaging and molecular techniques will yield a better understanding of the exact mechanisms invoked over the study duration (Carter et al. 2015).

Pericardial effusion is a characteristic of pericardial disease, which is common after exposure to radiation (Yusuf et al. 2011). Studies have also shown that PCE can lead to varying degrees of cardiac tamponade, which negatively impacts cardiac function (Khandaker et al. 2010). Further analysis using echocardiography is needed to explore the relationship between heart injury discussed above and the development of PCE.

DISCUSSION

Radiation-induced damage to the lung and heart is dose- and time-dependent and defined by organ-specific time-to-onset, severity, progression of damage and resolution (Garofalo et al., 2014a). Furthermore, the onset of clinical indices of lung injury initiates administration of trigger-based medical management such as dexamethasone, which can mitigate damage throughout the study duration. The ability to assess these dose- and time-dependent parameters in a longitudinal manner will allow a clear definition of the time course of radiation damage and its mitigation by medical management and MCM. Analysis provides insight into the evolution of damage to each organ as well as the interaction of each organ in establishing the time course of injury and dysfunction. The published literature on CT and EC imaging of normal macaques and those subjected to potentially lethal doses of acute radiation are minimal.

Establish a database

CT and EC provide non-invasive, longitudinal imaging of damage to the lung and heart. The ability to use these imaging modalities is dependent on establishing expertise and a database of key primary and secondary parameters in normal rhesus macaques. Healthy, age-matched rhesus macaques were used to establish a contemporary database for key parameters that will provide evidence of organ-specific dysfunction along a concurrent timeline, post lethal radiation exposure.

Computed tomography

It is imperative to utilize CT-based radiographic imaging and analysis to obtain the most accurate longitudinal, quantitative assessment of radiation-induced lung injury. A critical variable of the database is establishing the normal tissue range, in terms of HU. There are several published methods for lung segmentation using a HU range in rhesus macaque models (Garofalo et al. 2014b; Mohindra et al. 2015; Solomon et al. 2014). Solomon et al

initially used a HU range of −980 to −135 as the inclusion range for normal lung parenchyma at baseline and used statistical analysis to obtain volumes of damaged lung in follow-up exams (Solomon et al. 2014). A previous study by Garofalo et al. a HU range of −880 to −200 for lung segmentation and evaluation of lung injury over time post irradiation (Garofalo et al. 2014b). The same HU range was used for all initial rhesus macaque CT scans herein. Qualitative analysis of lung CT images however, revealed that areas of damaged lung appeared to be consistently included in this range, potentially compromising the integrity of our index of damage to normal tissue ratios (Fig. 2). This potential discrepancy highlighted the need for reanalyzing the concept of the normal lung HU range. More personalized methods have been proposed for adjusting the HU cutoff values for normal lung to more accurately determine injury progression over time (Mohindra et al. 2015; Solomon et al. 2014).

Echocardiography

Rhesus macaques are commonly used in cardiovascular research, and normal reference values have been published (Korcarz et al. 2008). Korcarz et al established normal values for 2 to 10 year old rhesus macaques that are similar, overall, to the values of the rhesus used herein. However, the age range is broad and the average values may be affected by age-dependent changes in cardiac function. Tang et al published data on two age ranges of rhesus macaques, 7 to 8 years and 17 to 20 years and confirmed that measurements of left ventricle size increased as the rhesus aged. As age increased from young adult to mature adult, the systolic function of the heart decreased, which caused a compensatory reflex to increase heart activity with a resultant hypertrophy (Tang et al. 2008). The radiation research community has characteristically used rhesus macaques in the juvenile to young adult age range for over six decades (MacVittie et al. 2015). This persistent trend toward the younger age range may explain why the left ventricular measurements from the naïve rhesus herein are similar to the younger group of Tang (Tang et al. 2008). The rhesus macaques used in this study were three to six years of age which underscores the critical requirement for an age-matched normal database and use of pre-irradiation values for each animal. While both studies contain similar values to the rhesus used herein, the lack of age-matched controls in the radiation field dictated that a more relevant dataset be established.

CT- and EC-based imaging of irradiated macaques

Longitudinal analysis of the CT scan data from baseline through 180 DPI or euthanasia provided an opportunity to assess the evolving changes of RILI and pericardial injury. This model allows objective quantification of the impact of radiation injury by measurement of changes suggestive of PF, PE and PCE. Computed Tomography scans showing PF and large quantities of PE on 30 DPI suggested the mechanism of lung injury may occur prior to 30 DPI (Fig. 6). Additionally, the observable progression of PF, even at 180 DPI, suggests that RILI is a persistent, on-going condition. Future studies may examine CT scans prior to 30 DPI and after 180 DPI to further evaluate the onset and duration of the mechanism involved in radiation-induced lung injury. The differences between the amounts of PE:TLV at 30 DPI and 180 DPI suggest PE is an early effect of radiation-induced lung injury (Table 2). Survivors and non-survivors both demonstrated an overall upward trend in PF over the 180 day time course (Fig. 6). As expected, lower percentages of PF and PE were observed in

survivors than non-survivors at similar time points (Figs. 5.a.b and 6). Considering the same radiation dose was delivered to both cohorts, this highlights the individual variations in susceptibility to radiation-induced injury. The increase in PF:TLV observed over the 180 day study course indicated a progressive injury to the lung. Dexamethasone and furosemide administration may have reduced the PF:TLV that occurred over the course of the study.

Due to the observation of various morphological changes in the right side of the heart as well as these increases in PF and PE, the EC examination will be expanded to include increased analysis of the right side of the heart. Dimensions and volumes of the right ventricle and atrium will be included in addition to pulmonary artery diameter and other right heart measurements. Future analysis will also include tissue Doppler-derived strain imaging on the left and right ventricle in order to assess myocardial mechanics on a subclinical level.

The CT and echocardiogram data are essential pieces to understanding the longitudinal development of severe multi-organ injury after high-dose, acute radiation exposure. However, we are limited in our ability to understand the specific pathology occurring using CT and EC alone. These noninvasive, multi-modal imaging methodologies will be correlated with numerous clinical, tissue and plasma/sera-based techniques, to include: longitudinal clinical observations and parameters such as non-sedated respiratory rate, SpO_2, blood pressure, time-based procurement at necropsy of tissue for MALDI-MSI, molecular analysis, histochemistry, histo-pathology, PE and PCE analysis and plasma analysis for cytokines and biomarkers.

Cautionary Notes: potential problems and solutions

The rhesus macaque animal model for radiation-induced injury to the lung and heart presented certain challenges. CT techniques evaluating the lung require the patient to hold their breath and remain still, which is difficult in an animal model. Studies have demonstrated that a lack of breath-holding techniques lead to inconsistent lung volume measurements (Solomon et al. 2014). This problem was remedied by relating measurements of damage (PF, PE) against total lung volume. With this method, variations in lung volumes between scans are marginalized. Motion artifacts created by respiration are a problem that must be considered when identifying organ borderlines on CT and echocardiograms. The use of dexamethasone has been demonstrated to have an effect on the radiographic appearance of injury in the lungs, which is a confounding variable when attempting to identify patterns of lung PF and PE. A potential way of circumventing this issue would be performing a future study which eliminates the use of dexamethasone, expanding the understanding of the timeline of RILI mechanisms. The lack of contrast media adds to the difficulty of identifying pulmonary vessels and structures of the heart on CT scans.

Other difficulties also exist in the realm of EC. For example, when lung injury develops from the delayed effects of radiation, increased tissue densities develop and adherences can occur, which block the acoustic window normally used by the technician. In this situation, an alternate window may be obtained by moving the transducer to a different position on the chest, which complicates the echocardiographic procedure and may result in suboptimal images. Rhesus macaques typically have an increased heart rate relative to larger animal

models which can cause problems in data analysis. For example, an elevated heart rate can cause summation of the mitral E and A waves and make observations of other anatomical features more difficult.

SUMMARY

Computed tomography and echocardiography have the potential to provide invaluable information about the progression of radiation-induced heart and pulmonary damage. The MCART consortium have developed rhesus macaque animal models that allow for longitudinal analysis of these modalities that will hopefully reveal clinically relevant symptoms as well as discover the active mechanisms of organ injury. Standardization of these techniques was performed and baseline databases were established for comparison to radiation treatment groups. Future studies will continue to develop protocols to further investigate the radiation-induced syndromes in the heart and lung.

REFERENCES

Carter CL, Jones JW, Jackson IL, Vujaskovic Z, Kearney S, Barrow K, Gibbs A, Kieta K, Taylor-Howell C, Farese AF, MacVittie TJ, Kane MA. Application of MALDI-MSI to identify biomarkers of radiation-induced lung injury and medical countermeasure development of AEOL10150. Health Phys. 2015 in press.

Crawford LM, Food and Drug Administration. New Drug and Biological Drug Products; Evidence Needed to Demonstrate Effectiveness of New Drugs When Human Efficacy Studies Are Not Ethical or Feasible. 21 CFR Pt. 314 and 601. Federal Register. 2002; 67:37988–37998. [PubMed: 12049094]

Food and Drug Administration. Guidance for Industry: Product Development Under the Animal Rule. US Department of Health and Human Services, Center for Drug Evaluation and Research (CDER), and Center for Biologics Evaluation and Reserach (CBER); 2014. p. 1-48.

Garofalo M, Bennett A, Farese AM, Ward A, Taylor-Howell C, Cui W, Gibbs A, Lasio G, Jackson WI, MacVittie TJ. The delayed pulmonary syndrome following acute high-dose irradiation: A Rhesus macaque model. Health Physics. 2014a; 106:1, 56–72. [PubMed: 24276545]

Garofalo M, Bennett A, Farese AM, Harper J, Ward A, Taylor-Howell C, Cui W, Gibbs A, Lasio G, Jackson W III, MacVittie TJ. The delayed pulmonary syndrome following acute high-dose irradiation: a rhesus macaque model. Health Phys. 2014b; 106:56–72. [PubMed: 24276550]

Garofalo MC, Ward AA, Farese AM, Bennett A, Taylor-Howell C, Cui W, Gibbs A, Prado KL, MacVittie TJ. A pilot study in rhesus macaques to assess the treatment efficacy of a small molecular weight catalytic metalloporphyrin antioxidant (AEOL 10150) in mitigating radiation-induced lung damage. Health Phys. 2014c; 106:73–83. [PubMed: 24276551]

Geraci JP, Mariano MS, Jackson KL, Taylor DA, Still ER. Effects of dexamethasone on late radiation injury following partial-body and local organ exposures. Radiat Res. 1992; 129:61–70. [PubMed: 1530802]

Ghobadi G, van der Veen S, Bartelds B, de Boer RA, Dickinson MG, de Jong JR, Faber H, Niemantsverdriet M, Brandenburg S, Berger RFM, langendijk M, Coppes RP, van Luijk P. Physiological interaction of heart and lung in thoracic irradiation. Int'l J Radiat Oncol Biol and Physics. 2012; 84(5):e639–e646.

Gross NJ. Radiation pneumonitis in mice. Some effects of corticosteroids on morality and pulmonary physiology. J Clin Invest. 1980; 66:504–510. [PubMed: 7400326]

Gross NJ, Narine KR, Wade R. Protective effect of corticosteroids on radiation pneumonitis in mice. Radiat Res. 1988; 113:112–119. [PubMed: 3340715]

Hansson K, Häggström J, Kvart C, Lord P. Left atrial to aortic root indices using two-dimensional and M-mode echocardiography in Cavalier King Charles Spaniel with and without left atrial enlargement. Veterinary Radiology & Ultrasound. 2002; 43(6):568–575. [PubMed: 12502113]

Jones JW, Scott AJ, Tudor G, Xu PT, Jackson IL, Vujaskovic Z, Booth C, MacVittie TJ, Ernst RK, Kane MA. Identification and quantitation of biomarkers for radiation-induced injury via mass spectrometry. Health Phys. 2014; 106:106–119. [PubMed: 24276554]

Khandaker MH, Espinosa RE, Nishimura RA, Sinak LJ, Hayes SN, Melduni RM, Oh JK. Pericardial Disease: Diagnosis and Management. Symposium on Cardiovascular Diseases. Symposium on Cardiovascular Diseases, Mayo Clinic Proceedings. 2010; 85(6):572–593.

Korcarz CE, Padrid PA, Shroff SG, Weinert L, Wang RM. Doppler echocardiographic reference values for healthy rhesus monkeys under ketamine hydrochloride sedation. J Med Primatol. 2008; 26(6):287–298. [PubMed: 9438222]

Lang RM, Badano LP, Mor-Avi V, Afilalo J, Armstrong A, Ernande L, Flachskampf FA, Foster E, Goldstein SA, Kuznetsova T, Lancellotti P, Muraru D, Picard MH, Rietzschel ER, Rudski L, Spencer KT, Tsang W, Voigt JU. Recommendations for cardiac chamber quantification by echocardiography in adults: an update from the American Society of Echocardiography and the European Association of Cardiovascular Imaging. J Am Soc Echocardiogr. 2015; 28(1):1–39. e14. [PubMed: 25559473]

Lang RM, Bierig M, Devereux RB, Flachskampf FA, Foster E, Pellikka PA, et al. Recommendations for chamber quantification: a report from the American Society of Echocardiography's Guidelines and Standards Committee and the Chamber Quantification Writing Group, developed in conjunction with the European Association of Echocardiography, a branch of the European Society of Cardiology. J Am Soc Echocardiogr. 2005; 18:1440–1463. [PubMed: 16376782]

MacVittie TJ, Bennett A, Booth C, Garofalo M, Tudor G, Ward A, Shea-Donohue T, Gelfond D, Mcfarland E, Jackson W III, Lu W, Farese AM. The prolonged gastrointestinal syndrome in rhesus macaques: the relationship between gastrointestinal, hematopoietic, and delayed multi-organ sequelae following acute, potentially lethal, partial-body irradiation. Health Phys. 2012; 103:427–453. [PubMed: 22929471]

MacVittie TJ, Farese AM, Jackson WI. The hematopoietic syndrome of the acute radiation syndrome in rhesus macaques: A systematic review of the lethal dose response relationship. Health Phys ;. 2015 in press.

Mohindra, P.; Barrow, K.; Kieta, K.; Parker, J.; De Faria, E.; Taylor-Howell, C.; Dobbin, T.; Gibbs, A.; Farese, AM.; MacVittie, TJ. Use of Computed tomography (CT) scan to Assess Efficacy of Mitigators of Radiation-induced Lung Injury (RILI): A Rhesus Macaque Whole Thoracic Lung Irradiation (WTLI) Model. American Society for Radiation Oncology (ASTRO) 2015 Annual Meeting; 2015. 2015

Scott AJ, Jones JW, Orschell CM, MacVittie TJ, Kane MA, Ernst RK. Mass spectrometry imaging enriches biomarker discovery approaches with candidate mapping. Health Phys. 2014; 106:120–128. [PubMed: 24276555]

Solomon, J.; Johnson, R.; Douglas, D.; Hammound, D. New Image Analysis Technique for Quantitative Longitudinal Assessment of Lung Pathology on CT in Infected Rhesus Macaques. Computer-Based Medical Systems (CBMS), 2014 IEEE 27th International Symposium; 2014. p. 169-172.

Quiñones MA, Otto CM, Stoddard M, Waggoner A, Zoghbi WA. Recommendations for quantification of Doppler echocardiography: a report from the Doppler Quantification Task Force of the Nomenclature and Standards Committee of the American Society of Echocardiography. J Am Soc Echocardiogr. 2002; 15(2):167–84. [PubMed: 11836492]

Tang H, Wang LL, Cheng G, Wang L, Li S. Evaluation of the cardiovascular function of older rhesus monkeys by ultrasonography. J. Med Primatol. 2008; 37(2):101–108. [PubMed: 18333921]

Yusuf SW, Sami S, Daher IN. Radiation-Induced Heart Disease: A Clinical Update. Cardiology Research and Practice. 2011

van Luijk P, Novakova-Jiresova A, Faber H, Schippers JM, Kampinga HH, Meertens H, Coppes RP. Radiation damage to the heart enhances early radiation-induced lung function loss. Cancer Res. 2005; 65(15):6509–6511. [PubMed: 16061627]

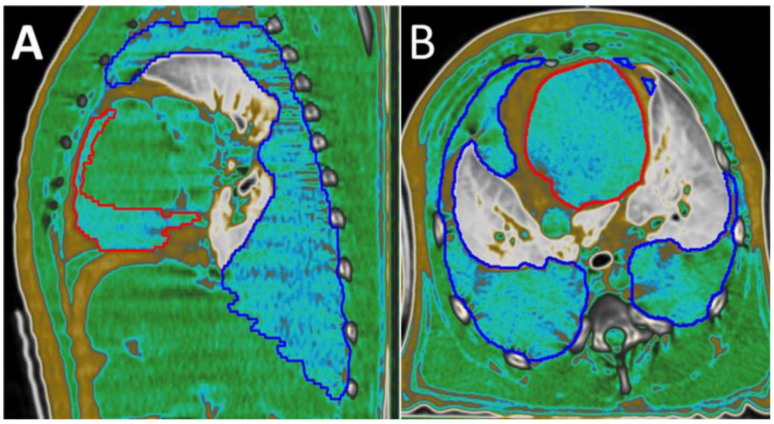

Figure 1.

CT image of NHP lung. Sagittal (A) and transverse (B) images from the same animal demonstrating the MIM® software HU Fat-Water-Tissue viewing window.

The red outline represents pericardial effusion and the dark blue outline representing pleural effusion. Both outlines surround areas of characteristic blue fluid. Yellow/gold appears around the outer edges representing subcutaneous fat and in between the red and blue lines in the center representing fat around the pericardium. Cardiac and back muscle tissue is shown in green. Lung tissue is displayed on a gray scale.

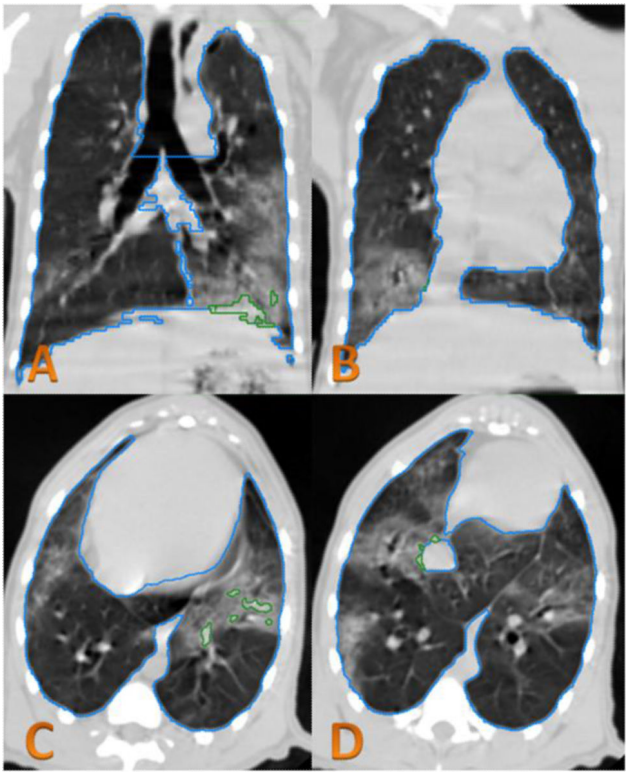

Figure 2.
CT analysis of irradiated NHP.
In the CT images obtained at 179 DPI, lung injury can be seen in the left lower lobe (image A,C) and the lower right lobe (image B,D). The green contour lines in the left lower lobe demonstrate lung injury that is excluded from the NLV using the conventional HU range of −880 to −200. This shows that not all of the visualized CT changes of lung injury were excluded from the NLV. The blue contour line is considered total lung volume.

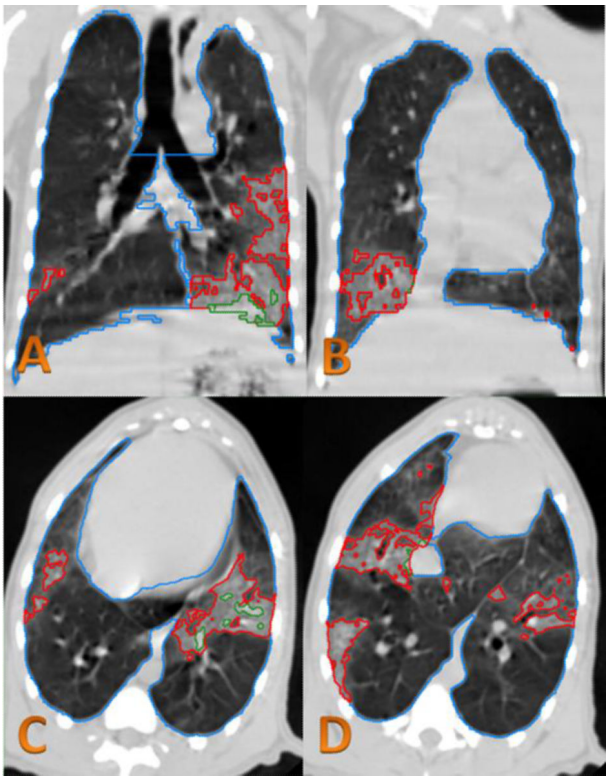

Figure 3.
CT analysis of irradiated NHP.
In the CT images obtained at 179 DPI from the same slice location as Figure 6, the red contour lines are the lung injury excluded from NLV using the HU range limit (−880 to −445). The green contour lines are the lung injury excluded from NLV using the old HU range limit (−880 to −200). The blue contour line is total lung volume.

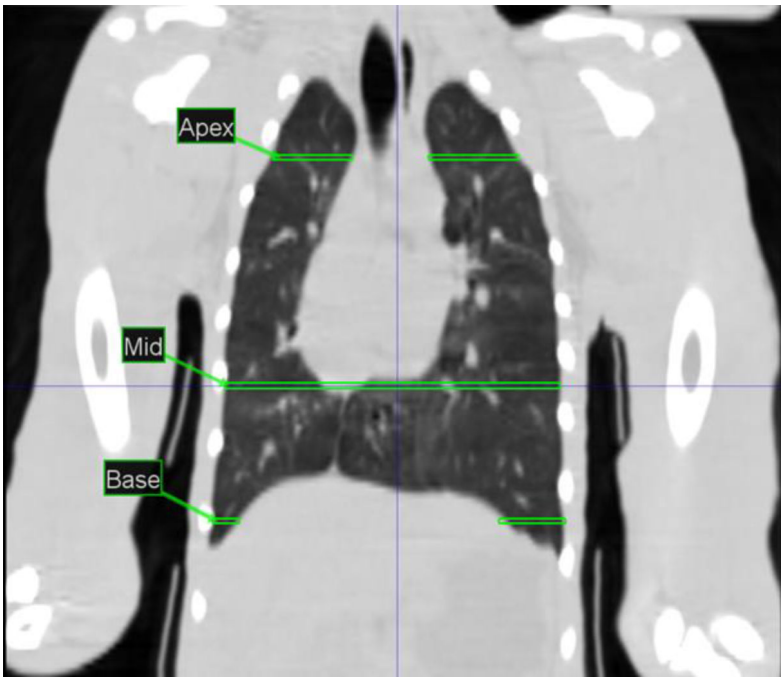

Figure 4.
Coronal View of baseline NHP indicating approximate areas where serial CT images labeled Apex, Mid and Base were acquired.

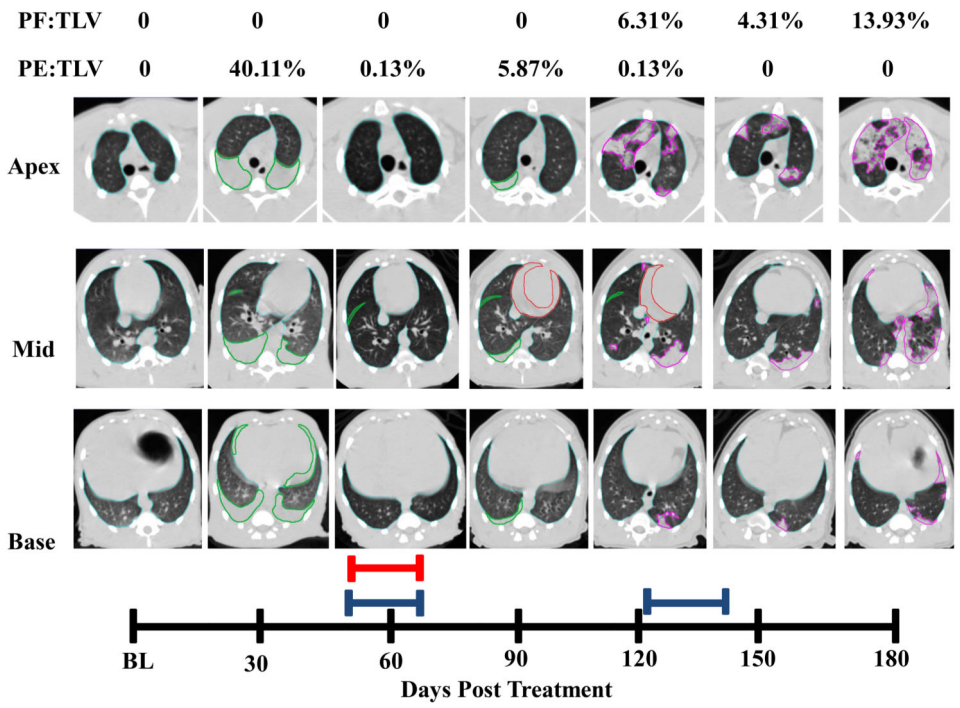

Figure 5.a.

Longitudinal CT analysis of a NHP exposed to 10.74 Gy WTLI, at baseline and followed every 30 days through the end of study at 180 DPI.

Transverse images were obtained taken at Apex, Mid and Base of lungs (Figure 4). Total Lung Volume (TLV) is outlined in light blue, pleural effusion (PE) in green, pericardial effusion (PCE) in red and pneumonitis/fibrosis (PF) in pink. The red bar represents one course of Furosemide administered 56-62 DPI for the presence of abdominal swelling as per veterinary request. The blue bars represent two courses of Dexamethasone administered DPI 54-62 and 121-146 as per study protocol. Pleural Effusion was observed 30-120 DPI. Pericardial Effusion was observed on day 90 at 21.68mL and at day 120 at 9.77mL. Pneumonitis/Fibrosis was observed 120-180 DPI.

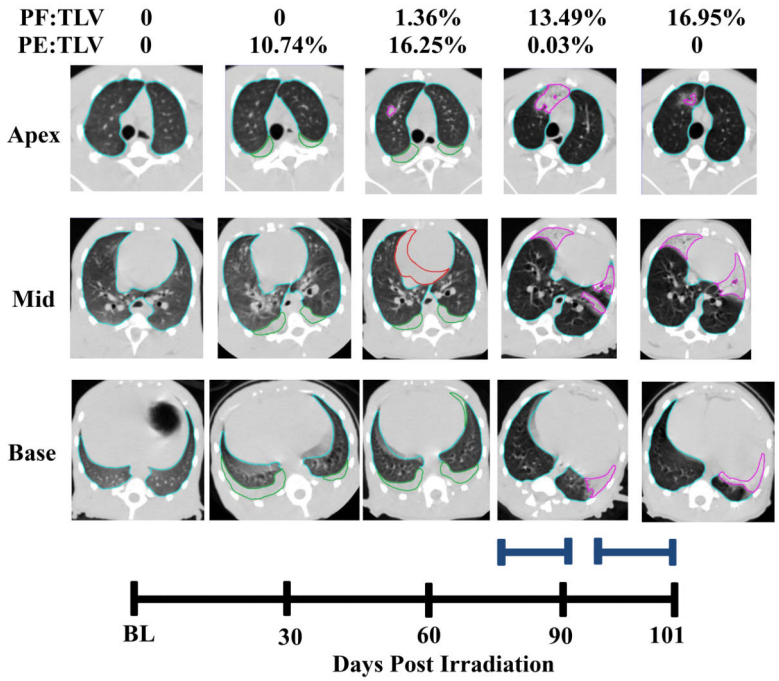

Figure 5.b.

Longitudinal CT analysis of a NHP exposed to 10.74 Gy WTLI, at baseline and followed every 30 days through to early euthanasia on day 101 due to study criteria.

Transverse images were obtained at Apex, Mid and Base of lungs (Figure 4). Total Lung Volume (TLV) is outlined in light blue, pleural effusion (PE) in green, pericardial effusion (PCE) in red and pneumonitis/fibrosis (PF) in pink. The blue bars represent two courses of Dexamethasone administered DPI 79-91 and 93-101 as per study protocol. Pleural Effusion was observed 30-90 DPI. Pericardial Effusion was observed on day 60 at 13.08mL.

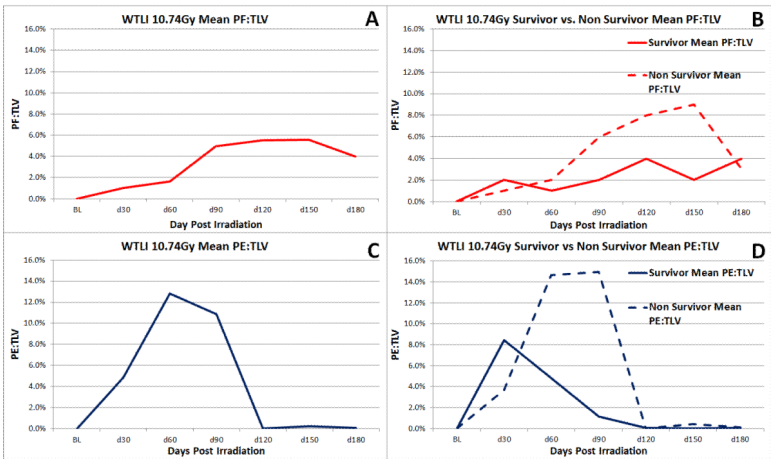

Figure 6.

Mean values for PF:TLV and PE:TLV are shown above.

(A) shows overall mean PF:TLV, (B) shows mean PF:TLV of survivors and non-survivors, (C) shows mean PE:TLV, and (D) shows mean PE:TLV of survivors and non-survivors.

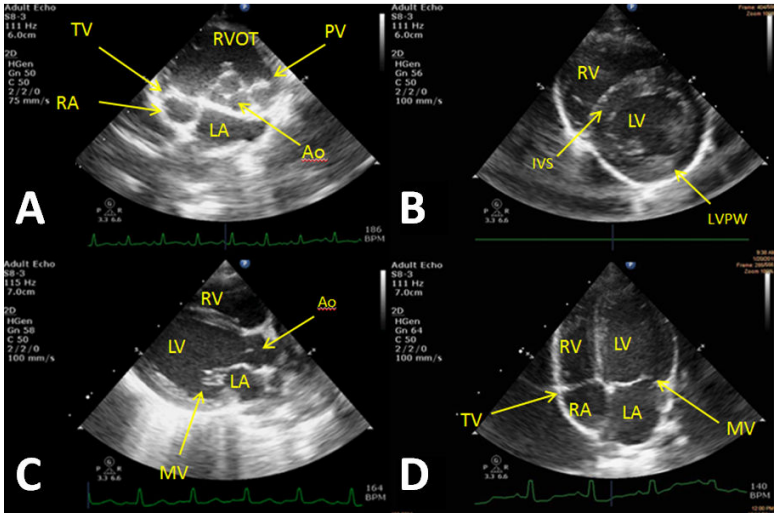

Figure 7.

Baseline images taken from different animals that represent the echocardiographic views from which measurements are taken.

A) Right parasternal short axis (RPSAX) at aortic valve level; Tricuspid (TV), aortic (Ao), and pulmonary valve (PV) are observed in addition to the right ventricle outflow tract (RVOT) and the left (LA) and right atria (RA). B) RPSAX at papillary level; left (LV) and right ventricular (RV) are observed in addition to the interventricular septum (IVS) and posterior wall (LVPW). C) RP Long axis; Left and right ventricle observed with additional views of the aorta and mitral valve (MV). D) Left parasternal apical four chamber view; All four chambers of the heart are observed in addition to the mitral and tricuspid valves.

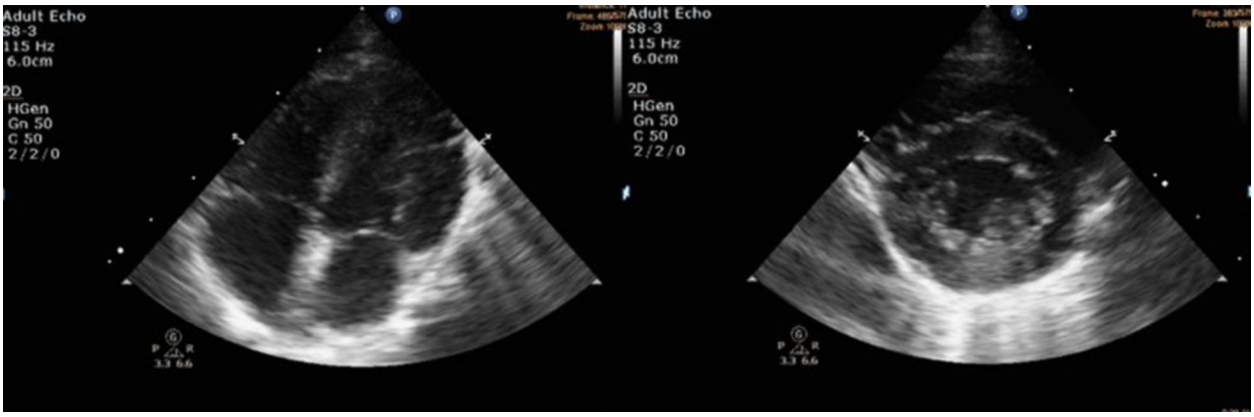

Figure 8.

Echocardiography of rhesus macaques exposed to WTLI at 10.74Gy (an approximate LD70/180).

Images were taken at 151 DPI. The image on the left shows mild right atrium enlargement, taken from the apical four chamber view. The image on the right shows mild right ventricle dilation.

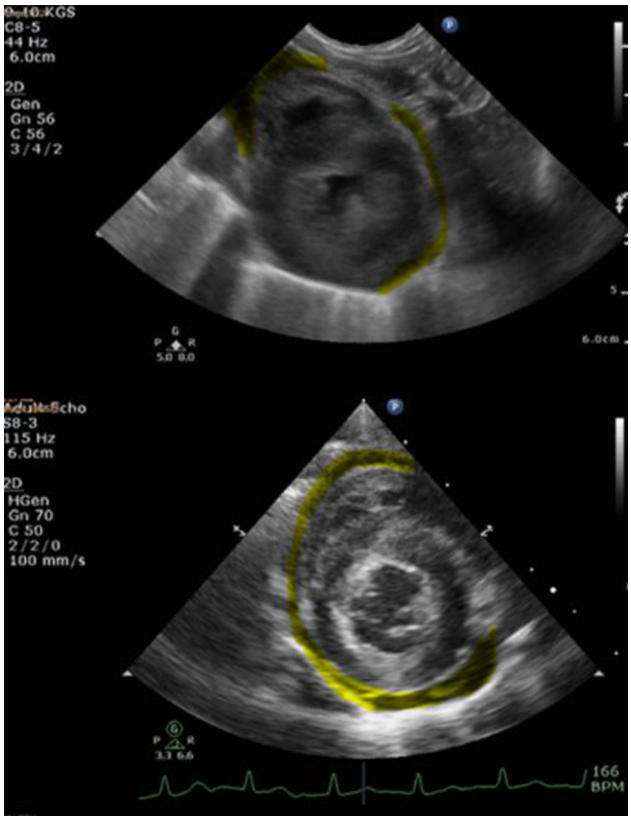

Figure 9.

Echocardiography of rhesus macaques exposed to WTLI.

Top image. NHP received WTLI (10.74Gy). Images taken at 95 DPI. Left ventricle hypertrophy was observed with pericardial effusion highlighted in yellow. Bottom image. NHP received 10Gy using the PBI/BM2.5 protocol. The image was taken at 88 DPI. Left ventricle hypertrophy and pericardial effusion observed. Both images taken from RPSAX view.

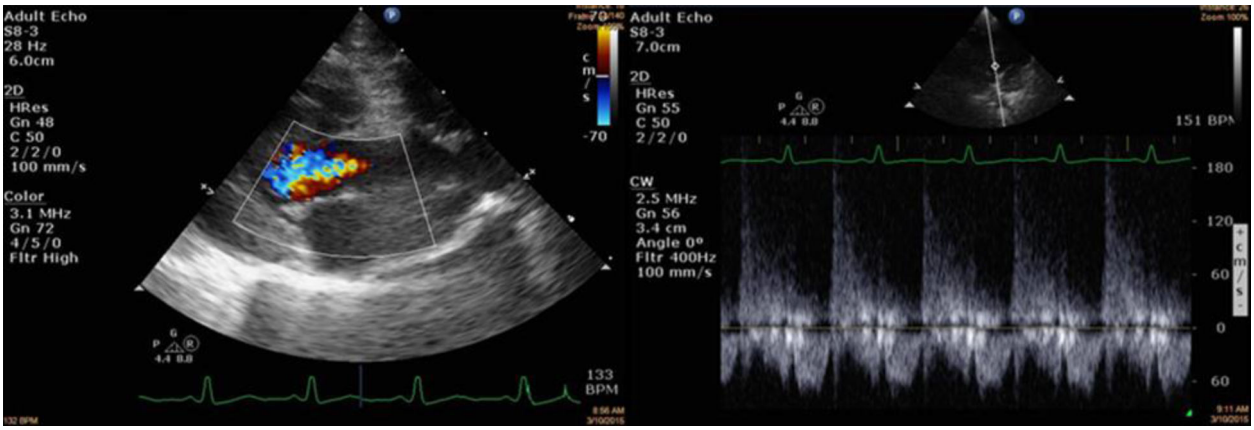

Figure 10.

Echocardiography of rhesus macaques exposed to PBI/BM2.5 protocol.

NHP received PBI/BM2.5 (10 Gy). Images were taken at 134 DPI. The image on the left was taken from the RPLAX view and shows aortic regurgitation. The right image is continuous wave Doppler across the aortic valve showing the peak velocity of the regurgitant jet from the leaky valve.

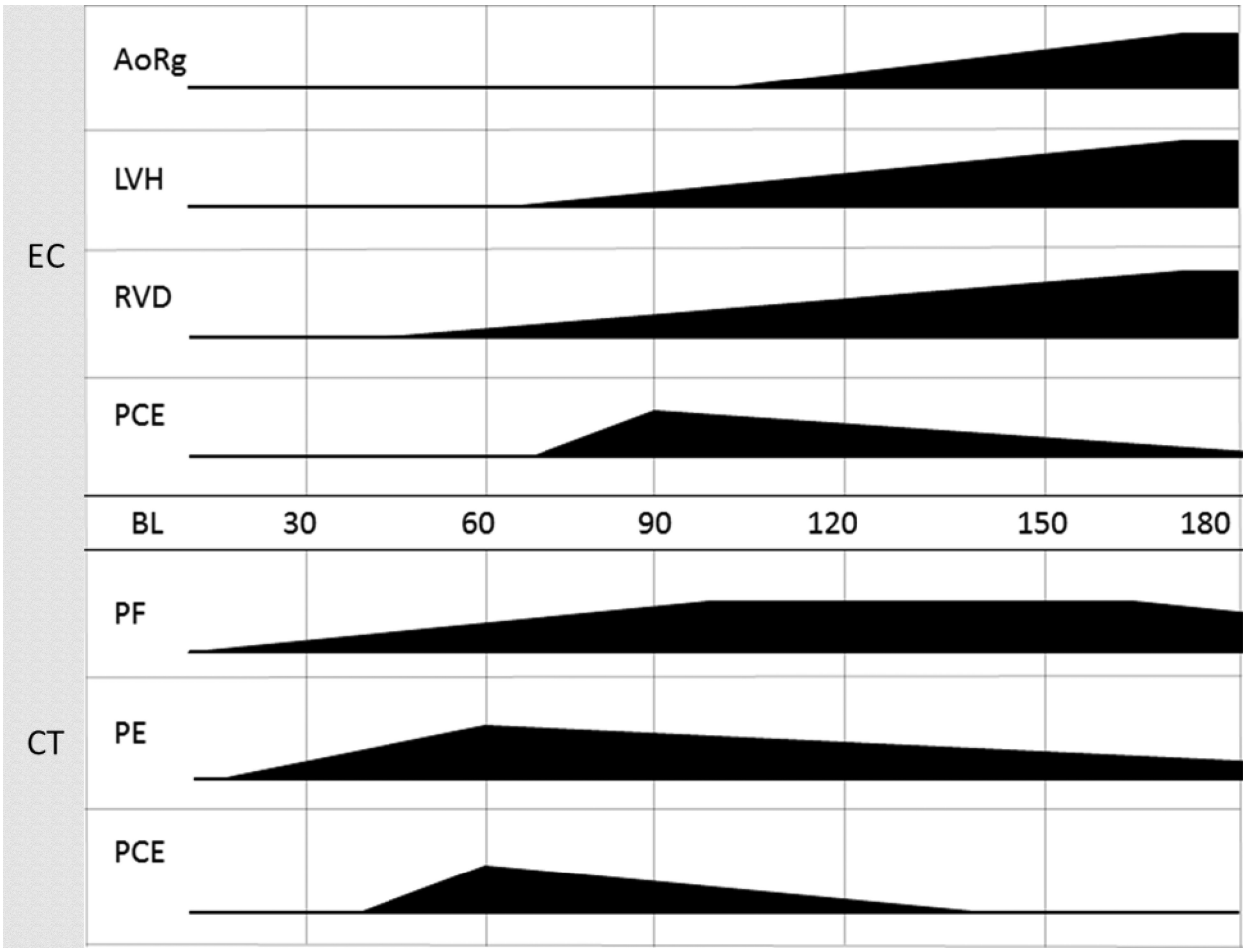

Figure 11.

Making the connection: Time of onset, progression, and severity of lung and cardiac tissue injuries.

The figure represents organ-specific injury initiated at time of radiation and progression to time of onset. Multimodal imaging occurs at 30 day intervals and impacts our ability to correctly identify the duration of the latent period. Subject-based trigger-to-treat medical management also impacts the severity and progression of organ injury. Given these variables the data base suggested certain trends of tissue damage to both organs. Pulmonary fibrosis/pneumonitis (PF) and pleural effusion (PE) first appear at 30 DPI. PF increased throughout study without resolution at 180 DPI. PE spiked in early time points and persisted in some NHP for the study duration. Pericardial effusion (PCE) viewed by computed tomography is observed from 60 DPI to 120 DPI. Cardiac damage appeared later. Aortic regurgitation (AoRg) first appeared at 120 DPI and increased until study conclusion. Left ventricle hypertrophy (LVH) first appeared at 90 DPI and progressed to the end of study. Right ventricle dilation (RVD) first appeared at 60 DPI and worsened throughout study duration. PCE first appeared at 90 DPI and diminished in volume throughout the study as seen by echocardiography (EC).Pulmonary-DEARE appeared to be more sensitive to acute radiation-induced injury than cardiac-DEARE relative to time of onset.

Table 1

Radiographic analysis of lung volume in rhesus macaque. The average total lung volume (TLV) established in volume (mL) and Hounsfield units (HU) from 40 normal baselines NHP. The mean of the average HU value for forty naïve rhesus macaques CT scans was calculated in addition to the average lung volume. Standard deviation, minimum and maximum was also calculated for each.

	Average of NHP mean TLV HU value	Lung volume (mL)
n =	40	40
Mean	−611.82	249.89
SD	48.07	42.20
Max	−522.55	343.78
Min	−706.06	183.49

Table 2

Twenty rhesus macaques exposed to WTLI 10.74Gy evaluated over 180 days using CT scans to obtain incidence of PF, PE and PCE. Decreasing n number related to rhesus macaques that met euthanasia criteria through course of study.

WTLI 10.74Gy Incidence of PF, PE and PCE						
DPI	**30**	**60**	**90**	**120**	**150**	**180**
n=	20	16	13	11	8	5
Incidence of PF	20.0%	43.8%	76.9%	100.0%	100.0%	80.0%
Incidence of PE	60.0%	50.0%	23.1%	54.5%	50.0%	40.0%
Incidence of PCE	0.0%	37.5%	15.4%	9.1%	0.0%	0.0%

Table 3

Left Ventricular Function and volume as measured by echocardiography in baseline rhesus macaques. Ejection fraction (EF), fractional shortening (FS), end diastolic volume (EDV), end systolic volume (ESV), and stroke volume (SV) of the left ventricle.

	EF (%)	FS (%)	LV Mass (g)	EDV (ml)	ESV (ml)	SV (ml)
n =	32	32	32	32	32	32
Mean	72.29	39.22	16.25	12.06	3.36	8.70
SD	6.60	5.60	2.99	3.61	1.40	2.65
r	0.17	0.19	0.19	0.24	0.04	0.30
Max	88.20	55.40	22.40	18.40	6.93	13.88
Min	59.10	29.50	11.10	5.45	1.38	3.85

Table 4

Left heart dimensions as measured by echocardiography in baseline rhesus macaques. Interventricular septum (IVS), Left ventricle interior diameter (LVID), left ventricular posterior wall (LVPW) measurements taken in end diastole and systole. Left atrium and aortic diameter ratio as measured by distance in end diastole (LA/Ao).

	IVSd (cm)	LVIDd (cm)	LVPWd (cm)	IVSs (cm)	LVIDs (cm)	LVPWs (cm)	Aor Diam (cm)	LA Diam (cm)	LA/Ao
n =	32	32	32	32	32	32	32	32	32
Mean	0.55	1.94	0.48	0.76	1.18	0.71	0.99	1.32	1.33
SD	0.08	0.24	0.09	0.19	0.19	0.10	0.10	0.19	0.20
r	0.05	0.21	−0.11	0.12	0.04	0.14	0.19	0.13	0.03
Max	0.77	2.31	0.66	1.59	1.58	0.89	1.27	1.62	1.82
Min	0.43	1.44	0.30	0.53	0.86	0.50	0.80	1.00	0.97

Table 5

Doppler Echocardiography parameters in baseline rhesus macaques. Aortic valve max velocity and calculated pressure gradient (AV Vmax and max PG), Mitral valve E and A wave peak velocity and calculated pressure gradient (MV Peak E/A Vel and PG), mitral valve E and A wave ratio (MV E/A), pulmonary valve max velocity and calculated pressure gradient (PV Vmax and max PG).

	AV Vmax (cm/s)	AV Max PG (mmHg)	MV Peak E Vel (cm/s)	MV Peak E PG (mmHg)	MV Peak A Vel (cm/s)	MV Peak A PG (mmHg)	MV E/A	PV Vmax (cm/s)	PV Max PG (mmHg)
n =	29	29	28	28	28	28	28	31	31
Mean	84.59	2.92	85.17	2.95	49.54	1.02	1.77	94.95	3.66
SD	12.35	0.85	10.38	0.69	10.04	0.41	0.31	11.53	0.88
r	0.05	0.04	−0.17	−0.19	−0.23	−0.27	0.11	0.31	0.32
Max	109.00	4.74	101.00	4.09	71.00	2.02	2.47	118.00	5.56
Min	62.40	1.56	63.80	1.63	31.80	0.40	1.28	71.50	2.05

Table 6

Serial M-mode measurements of left ventricle geometry for NHP receiving 10 Gy PBI/BM2.5 radiation treatment.

DPI	IVSd (cm)	LVIDd (cm)	LVPWd (cm)	IVSs (cm)	LVIDs (cm)	LVPWs (cm)
BL	0.43	1.88	0.39	0.50	0.99	0.69
56	0.54	1.57	0.43	0.67	0.84	0.70
119	0.66	1.31	0.76	0.88	0.70	1.00
179	0.78	1.35	0.80	0.91	0.71	1.15